### Title

Effects of Lipid Tethering in Extremophile-Inspired Membranes on H+/OH− Flux at Room Temperature




### Journal

Biophysical Journal, 110(11)

### ISSN

0006-3495



### Authors

Schroeder, Thomas BH
Leriche, Geoffray
Koyanagi, Takaoki
et al.



### Publication Date

2016-06-01

### DOI

10.1016/j.bpj.2016.04.044

Peer reviewed

Biophysical *Journal*
Article

Biophysical Society

# Effects of Lipid Tethering in Extremophile-Inspired Membranes on $H^+/OH^-$ Flux at Room Temperature

Thomas B. H. Schroeder,[1,2] Geoffray Leriche,[3] Takaoki Koyanagi,[3] Mitchell A. Johnson,[4] Kathryn N. Haengel,[4] Olivia M. Eggenberger,[2,4] Claire L. Wang,[4] Young Hun Kim,[3] Karthik Diraviyam,[4] David Sept,[4] Jerry Yang,[3] and Michael Mayer[2,4,*]

[1]Department of Chemical Engineering, University of Michigan, Ann Arbor, Michigan; [2]Adolphe Merkle Institute, University of Fribourg, Fribourg, Switzerland; [3]Department of Chemistry and Biochemistry, University of California San Diego, La Jolla, California; and [4]Department of Biomedical Engineering, University of Michigan, Ann Arbor, Michigan

ABSTRACT This work explores the proton/hydroxide permeability ($P_{H+/OH-}$) of membranes that were made of synthetic extremophile-inspired phospholipids with systematically varied structural elements. A fluorescence-based permeability assay was optimized to determine the effects on the $P_{H+/OH-}$ through liposome membranes with variations in the following lipid attributes: transmembrane tethering, tether length, and the presence of isoprenoid methyl groups on one or both lipid tails. All permeability assays were performed in the presence of a low concentration of valinomycin (10 nM) to prevent buildup of a membrane potential without artificially increasing the measured $P_{H+/OH-}$. Surprisingly, the presence of a transmembrane tether did not impact $P_{H+/OH-}$ at room temperature. Among tethered lipid monolayers, $P_{H+/OH-}$ increased with increasing tether length if the number of carbons in the untethered acyl tail was constant. Untethered lipids with two isoprenoid methyl tails led to lower $P_{H+/OH-}$ values than lipids with only one or no isoprenoid tails. Molecular dynamics simulations revealed a strong positive correlation between the probability of observing water molecules in the hydrophobic core of these lipid membranes and their proton permeability. We propose that water penetration as revealed by molecular dynamics may provide a general strategy for predicting proton permeability through various lipid membranes without the need for experimentation.

## INTRODUCTION

Acidophilic archaea have adapted to thrive in environments with very low pH (1). These organisms often rely on the acidity of their habitats to survive; archaea of the *Picrophilus* family, for example, have an optimal exterior pH of 0.7 and cannot grow above pH 3.5 (2). A large pH gradient (ΔpH) across the cell membrane is necessary both to maintain a near-neutral internal pH and to drive vital cell functions such as energy transduction with membrane-bound ATPases, which use proton flux driven by ΔpH to drive ATP production (3,4).

Acidophiles have evolved a number of mechanisms to maintain a gradient of several pH units across the cell membrane. To begin with, many such organisms express a variety of active transport systems to pump protons out of the cell (4–6); genetic evidence suggests that some form of proton efflux system exists in all acidophiles whose genomes have been sequenced (4). Additionally, unlike cells that grow in pH neutral environments, many acidophiles display a positive membrane potential that opposes proton influx (4). Finally, the cell membrane itself is often composed of lipids with unique structural characteristics thought to reduce proton permeability (4,7). These lipids usually contain ether bonds connecting the head glycerol group to the tails, increasing their chemical stability and potentially inhibiting the formation of transient hydrogen-bonded water chains compared to the ester bonds in standard phospholipids (8). Archaeal lipid tails often contain methyl branches in a repeating isoprenoid pattern, as well as cyclopentane and cyclohexane rings. Most unusually, many acidophile lipids are membrane-spanning structures with two tethered hydrophilic headgroups; typically, these are macrocycles with two tethering alkyl chains, but some have one tether and one free-hanging tail attached to each headgroup (9). Both the tethered/untethered ratio (10) and ring count (11–13) of lipids in thermoacidophilic archaea have been shown to increase with culture temperature, implying that these adaptations and the related biosynthetic pathways are related to heat stability (10,11). In addition, membranes formed from extracts of archaeal lipids are more resistant to

*Submitted October 15, 2015, and accepted for publication April 12, 2016.*

*Correspondence: michael.mayer@unifr.ch

Editor: Arne Gericke.

http://dx.doi.org/10.1016/j.bpj.2016.04.044

ΔpH relaxation than those formed from *Escherichia coli* extracts even at room temperature (7).

Passive permeation of protons across membranes in aqueous systems is mechanistically different and significantly faster than permeation of other polar or charged molecules, although the exact mechanism is still not known. In this context, it is important to note that discussion of "proton permeation" actually represents a discussion of the permeation of protons, hydroxide ions, or both, as it is practically impossible to distinguish between a flux of protons in one direction and a flux of hydroxide ions in the other. The proposed modes of $H^+/OH^-$ flux that have historically received the most attention tend to rely on the ability of protons to "hop" between hydrogen-bonded water molecules, an idea first described by de Grotthuss in 1805 (14). Despite this long history, the specifics of this mechanism are still being resolved (15), but most membrane $H^+/OH^-$ permeation models propose the formation of short-lived clusters or wires of water across the membrane (16–18). Paula et al. presented data consistent with this model in systems of liposome membranes with thin hydrophobic regions ($<$3.1 nm), whereas thicker hydrophobic regions ($\geq$3.4 nm) were better described by a solubility-diffusion mechanism involving $H_9O_4^+$ (19). In 2010, Nichols and Abercrombie proposed a five-step "transmembrane condensation model" in which a proton and a hydroxide anion spontaneously appear on either side of a membrane and interact electrostatically across the membrane; in rare cases, one species or the other overcomes its Born energy barrier and penetrates into the hydrophobic core, likely in the form of a cluster of water molecules (rendering it potentially consistent with the transient water wire hypothesis) (20). Whatever the mechanism, the permeation of protons or hydroxide ions is conventionally described by a permeability coefficient, $P_{H+/OH-}$, in units of cm $s^{-1}$, defined by Fick's law (Eq. 1):

$$J = P_{H^+/OH^-} \times \Delta C, \tag{1}$$

where $J$ (mol $m^{-2}$ $s^{-1}$) is the inward flux of solute across the membrane, $P_{H+/OH-}$ (m $s^{-1}$) is the permeability of the membrane, and $\Delta C$ (mol $m^{-3}$) is the concentration gradient across the membrane.

Widely varying values of $P_{H+/OH-}$ have been observed both between and within laboratories. Reported $P_{H+/OH-}$ values for membranes composed of the lipid 1-palmitoyl-2-oleoyl-*sn*-glycero-3-phosphocholine (POPC), for example, include values on the order of $10^{-1}$ cm $s^{-1}$ (21), $10^{-2}$ cm $s^{-1}$ (22), $10^{-5}$ cm $s^{-1}$ (23), and $10^{-7}$ cm $s^{-1}$ (24,25); these disparate values were all similarly obtained by subjecting liposomes to a stepwise ΔpH and observing proton flux over time. Mathai et al. attribute at least some of this orders-of-magnitude variability to differences in the size of the gradient imposed during the assays, prescribing the use of a small ΔpH of 0.5 (8). Recommendations such as this are sensible; there is a clear need for a standard, well-defined assay for permeation of $H^+/OH^-$ across membranes so that $P_{H+/OH-}$ values obtained by different groups can be compared. However, Kuyper et al. analyzed $H^+/OH^-$ permeation across hundreds of single vesicles in parallel and observed a high degree of variation in $P_{H+/OH-}$ between liposomes in the same experiment without observing correlation with liposome size or any other observable parameter, indicating that broad distributions of $P_{H+/OH-}$ values may be unavoidable (24). This result was obtained from ensemble measurements as well; van de Vossenberg et al. recorded a spread of nearly an order of magnitude in permeation rate constants in liposomes containing lipids from *Bacillus subtilis* (26).

In an attempt to obtain consistent readings of this notoriously fickle parameter, we have optimized an established liposome-based assay for $P_{H+/OH-}$ developed by Paula et al. that tracks the fluorescence decay of an encapsulated pH-sensitive dye in response to a step change in the external pH (19). To this end, we have developed a fitting procedure that incorporates empirical measurements of buffering activity and fluorescent response to pH taken during an internal calibration into an algorithm that fits the entire decay curve obtained during each experiment. We have also determined a concentration range in which the ionophore valinomycin is selective for $K^+$ over $H^+$ to eliminate the membrane potential that would arise from imposing a concentration gradient on a system with a single mobile ion while minimizing possible artifacts in the measured $H^+/OH^-$ permeability due to valinomycin-induced proton flux.

To make this study possible, we synthesized a series of extremophile-inspired lipids composed of two glycerophosphocholine heads connected by a membrane-spanning *n*-alkyl tether with each head ether-bonded to a phytanyl chain (T28, T32, and T36 (Fig. 1, *A–C*)), as well as several untethered lipids (U16, 1,2-di-O-phytanyl-*sn*-glycero-3-phosphocholine (Di-O-PhyPC), 1,2-diphytanoyl-*sn*-glycero-3-phosphocholine (DiPhyPC), and POPC (Fig. 1, *D–G*)) to seek answers to our questions about structure-permeability relationships of liposomes from pure lipid preparations at room temperature: First, how does the presence of a single tether between two lipid headgroups affect $P_{H+/OH-}$ compared to the absence of a tether? Second, how does the length of the tether affect $H^+/OH^-$ permeability when the lengths of the untethered phytanyl chains are kept constant at 16 carbons? And third, how does the $P_{H+/OH-}$ of an untethered lipid with a repeating isoprenoid methyl motif on one of its tails compare to that of a lipid with the methyl groups on both tails?

## MATERIALS AND METHODS

The lipids shown in Fig. 1, *A–D*, were synthesized as shown in the Supporting Material (Sections S3 and S4). POPC, DiPhyPC, and Di-O-PhyPC were from Avanti Polar Lipids (Alabaster, AL); pyranine was from Sigma-Aldrich (St. Louis, MO).

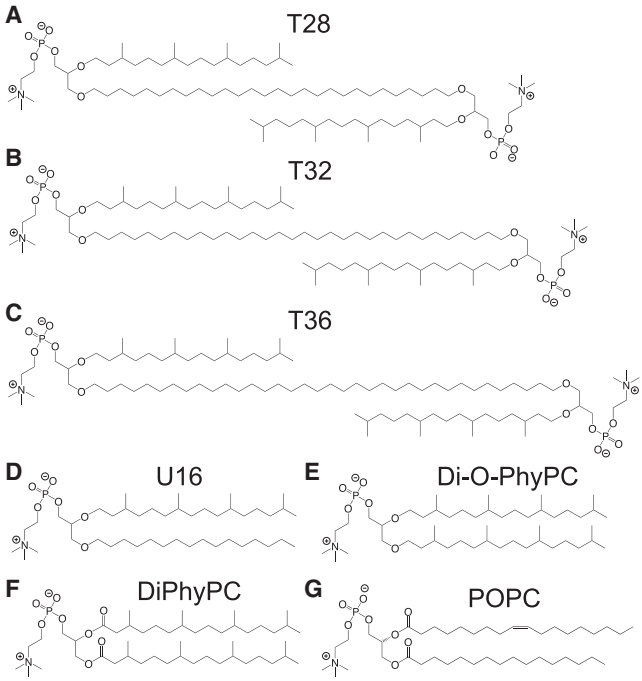


FIGURE 1 Extremophile archaea-inspired lipid structures examined in this work. (*A*) Lipid with a tether length of 28 carbons (T28). (*B*) Lipid with a tether length of 32 carbons (T32). (*C*) Lipid with a tether length of 36 carbons (T36). (*D*) Untethered lipid equivalent to half of T32 (U16). (*E*) 1,2-di-O-phytanyl-*sn*-glycero-3-phosphocholine (Di-O-PhyPC). (*F*) 1,2-diphytanoyl-*sn*-glycero-3-phosphocholine (DiPhyPC). (*G*) 1-palmitoyl-2-oleoyl-*sn*-glycero-3-phosphocholine (POPC).

## Preparation and sizing of unilamellar liposomes

We formed a homogeneous lipid film on the bottom of a 10 mL round-bottom flask via gentle rotary evaporation of a 1 mL solution of lipid in chloroform (10 mM for lipids with one headgroup and 5 mM for bipolar lipids). We hydrated the film with 1 mL of a buffered aqueous solution containing 50 $\mu$M pyranine, 50 mM $K_2SO_4$, 10 mM N-(2-acetamido)-2-aminoethanesulfonic acid, 10 mM 2-(*N*-morpholino)ethanesulfonic acid, 10 mM N-[Tris(hydroxymethyl)methyl]-2-aminoethanesulfonic acid, and 10 mM tricine, pH 7.25, and heated the flask to 37°C in a water bath for $\geq$3 h. After transferring the resulting solution of liposomes to an Eppendorf tube, we performed 15 freeze-thaw cycles in which we alternated between flash-freezing the solution in liquid nitrogen for 30 s and thawing it in a water bath at 45°C for 3 min.

Exercising care to avoid the formation of bubbles, we pushed the solution seven times through a polycarbonate membrane with pores of known diameter with a mini-extruder (Avanti Polar Lipids). We obtained the resulting size distribution of liposomes within the solution via dynamic light scattering (DLS) using a 90Plus particle sizer (Brookhaven Instruments, Holtsville, NY). We then pushed the liposome solution another 21 times through a polycarbonate membrane with pores of a diameter below the smallest diameters of the size distribution shown on the DLS readout (we usually used 80 nm pores) to minimize the probability of liposomes crossing the membrane without breaking into smaller vesicles, thereby maximizing the probability of obtaining a homogeneous solution of unilamellar liposomes (27). We determined the new size distribution using DLS and used the mode of the distribution to calculate the radius used in the fitting equation. We also determined via DLS that liposomes formed in this way did not undergo significant changes in size distribution for at least 3 days.

## Optimized fluorescence-based permeation assay

We removed all extravesicular pyranine by running the liposome solution sequentially through two PD-10 desalting columns (GE Healthcare, Little Chalfont, United Kingdom) with an eluent identical to the incubation buffer solution but without pyranine, collecting fractions of 1 mL each. We found that using one desalting column was insufficient and resulted in a significant concentration of pyranine remaining outside the vesicles. We transferred a 1 mL fraction containing liposomes to a cuvette, then added 1 $\mu$L of a solution of valinomycin (10 $\mu$M in dimethylsulfoxide (DMSO)) to reach a final concentration of 10 nM and mixed by gentle pipetting.

After 30 min, we measured the extravesicular pH of the solution with a calibrated Orion 5-Star pH meter (Thermo Scientific, Waltham, MA). We used a Fluorolog spectrofluorometer (Horiba Jobin Yvon, Edison, NJ) to collect fluorescence measurements over time. Every 2.5 s, the instrument collected one pH-invariant fluorescence intensity value by exciting the sample with a wavelength of 415 nm and collecting emission at 510 nm and one pH-dependent value by exciting at 450 nm and collecting at 510 nm (excitation and emission band pass, 1 nm; integration time, 0.5 s). Before imposing the $\Delta$pH, we collected an initial fluorescence measurement for 30 s to ensure that no discernible change in the fluorescence intensity was occurring over time at either excitation wavelength. We then added 10 $\mu$L of an aqueous solution of $H_2SO_4$ (250 mM) to the cuvette, mixed by pipetting up and down, and began collecting fluorescence data as quickly as possible, recording the duration that passed between acid addition and the start of fluorescence data collection. This addition of acid induced a pH change from 7.25 to ~6.75.

After the resulting fluorescence decay curve had been recorded, we added 0.67 $\mu$L of a solution of the protonophore nigericin in ethanol (100 $\mu$M) to render the vesicle membrane permeable to protons, mixed by pipetting up and down, measured and recorded the pH with a pH meter, and continued to record the fluorescence. We then proceeded to add five "calibration jumps" of 2 $\mu$L aqueous KOH solution (500 mM), measuring the pH and recording the fluorescence until a stable baseline was reached before moving to the next jump. The final pH of the vesicle solution was ~7.25.

After data collection was complete, we modified the time values of the fluorescence curves to reflect the delay between acid addition and the start of the fluorescence data and added a point at $t = 0$ corresponding to the initial fluorescent value measured before the pH jump. We then made scatter plots from the data collected during calibration, relating the pH, the ratio of the fluorescence intensities, $I_{450}/I_{415}$, and the added acid concentration, $[H^+]_{cross}$; we fit these plots with exponential functions to obtain empirical fitting parameters $A_1$, $A_2$, $x_1$, $x_2$, $y_1$, and $y_2$ (Fig. 2, *B* and *C*). Finally, we plotted $I_{450}/I_{415}$ versus time and fit the decay portion of the curve up to the addition of nigericin with Eq. 2 (derived in the Calculation section) (Fig. 2 *A*):

$$\frac{I_{ex450}}{I_{ex415}} = A_2\left(\frac{[H^+]_{f,o} - y_1}{A_1 - Ce^{\frac{3P_{H^+/OH^-}\left(y_1 - [H^+]_{f,o}\right)}{rx_1}t}}\right)^{-x_1/x_2} + y_2, \tag{2}$$

where $[H^+]_{f,o}$ is the exterior proton concentration during the main decay phase, obtained from the pH measured after nigericin is added; $A_1$ (mol m$^{-3}$), $A_2$ (unitless), $x_1$ (mol m$^{-3}$), $x_2$ (mol m$^{-3}$), $y_1$ (mol m$^{-3}$), and $y_2$ (unitless) are the empirical fitting parameters from the calibration fits (Fig. 2, *B* and *C*, explained in Calculation); $C$ (mol m$^{-3}$) is a constant of integration; $P_{H+/OH-}$ (m s$^{-1}$) is the $H^+/OH^-$ permeability; $r$ (m) is the most probable liposome radius as determined by DLS; and $t$ (s) is time. The parameters $C$ and $P_{H+/OH-}$ are allowed to vary during fitting.

## Atomic force microscopy on lipid monolayers

Liposomes composed of T28 and T36 were prepared by adding 10 $\mu$L of each lipid (10 mg/mL in an 80:20 chloroform/methanol solution) to

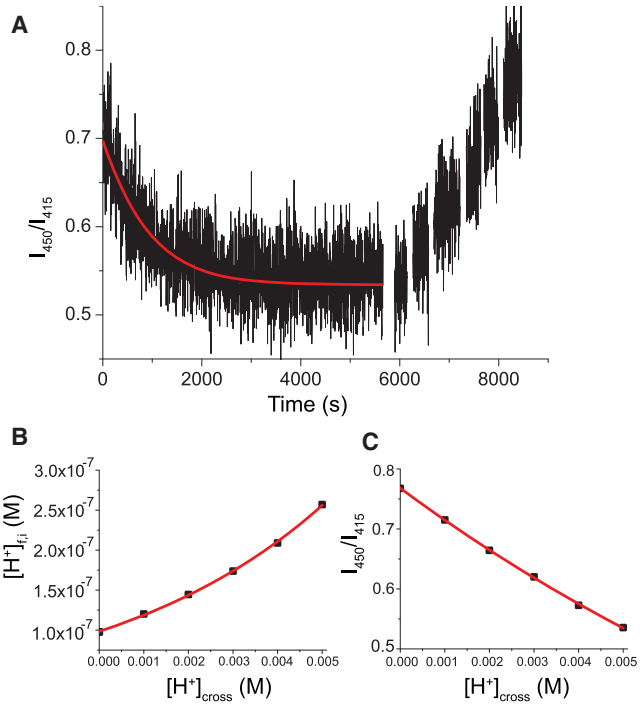


FIGURE 2 Determining proton permeability with liposomes that encapsulate the pH-sensitive, ratiometric fluorophore pyranine. (*A*) Fluorescence emission ratio $I_{450}/I_{415}$ as a function of time after addition of acid to impose a pH jump with a best curve fit using Eq. 2. Nigericin was added at ~5700 s; KOH was added during all subsequent breaks in the trace. (*B*) Dependence of $[H^+]_{f,i}$ as a function of $[H^+]_{added}$ with an exponential curve fit to the equation $[H^+]_{f,i} = A_1 e^{[H^+]_{cross}/x_1} + y_1$. (*C*) Dependence of the fluorescence emission ratio $I_{450}/I_{415}$ as a function of $[H^+]_{added}$ with an exponential curve fit to the equation $I_{450}/I_{415} = A_2 e^{[H^+]_{cross}/x_2} + y_2$. To see this figure in color, go online.

round-bottom flasks and removing the solvent by rotary evaporation; the lipid films were dried under high vacuum for ~1 h. An aqueous solution of 150 mM KCl and 10 mM HEPES at pH 7 was added to resuspend the lipids to a final lipid concentration of 0.1 mg/mL. The suspension was then incubated in a water bath at 50°C for 30 min. The solutions containing lipids were sonicated for 5 min to form liposome suspensions. The solutions were added to a mica substrate and incubated for 1 h. The liposomes were fused and ruptured on the mica substrate (28–30). To remove excess liposomes, the mica surfaces were rinsed 10 times with a 150 mM KCl solution.

Samples were imaged by multimode atomic force microscope using a Nanoscope IV controller (Bruker, Santa Barbara, CA). The tapping-mode images were acquired using silicon nitride cantilever tips submerged in buffer. A resonance frequency of ~8 kHz and drive amplitude under 100 mV were used (Asylum Research, Santa Barbara, CA). Nanoscope software was used for depth analysis to estimate the height of the lipid membranes.

## Molecular dynamics simulations

The structural models for the archaea lipids were constructed and minimized using Maestro (Schrödinger LLC, New York, NY). The modeled lipids all had an all-*trans* conformation along the hydrocarbon chain. The single lipid was then translated and rotated along the $x$ and $y$ directions to build a smaller model membrane system comprising 81 lipids. Upon running equilibration simulations (50 ns) on this smaller membrane model, the equilibrated small membrane model was replicated in the $x$ and $y$ axes to build a bigger membrane model of 729 total lipids (1458 in the case of U16). The dimensions of the bigger membrane models were in the range of 200 × 200 × 50 Å on average across the different membrane models. Visual molecular dynamics (VMD) (31) was used to make the translations and rotations of lipid in building the membrane. For POPC, we used the built-in membrane tool in VMD and produced a membrane of 1458 total lipids to match the sizes of the other systems. The simulation data from these larger membrane models were used for all subsequent simulations and calculations.

MD simulations for all membrane systems were performed for 100 ns after equilibration at pH 7, 300 K, and an ionic strength of 50 mM under the isothermal-isobaric (NpT) ensemble. The temperature was maintained by using the Nosé-Hoover chain method and the pressure was maintained at 1 atm. All the simulations were carried out using NAMD (32) in explicit water using TIP3P water models. The CHARMM36 lipid force field was used with a 10 Å cut-off for van der Waals with an 8.5 Å switching distance, and particle-mesh Ewald for long-range electrostatics. Analysis was carried out in the final 50 ns of the simulation.

All postsimulation trajectory analyses were carried out using R (http://www.R-project.org). The bending rigidity, $k_c$, was determined by decomposing the fluctuation in membrane height, $\langle |h_q|^2 \rangle$, in terms of the wave number, $q$, based on the equation $\langle |h_q|^2 \rangle = k_B T/2(1/k_c q^4 + 1/k_\theta q^2 + 1/k_\lambda)$ (33). The entropy of the individual lipids was determined using the Schlitter formula $Sk_B/2\ln \det[\mathbf{I} + (kTe^2/\hbar^2)\mathbf{M}\sigma]$ (34) where $\mathbf{M}\boldsymbol{\sigma}$ is the mass-weighted covariance matrix calculated from the simulations. Finally, the diffusion constants $D_1$ and $D_2$ were determined by fitting the mean-square displacement according to the formula (35)

$$\langle x(t)^2 \rangle = \frac{4D_1 t r_o^2}{r_o^2 + 4D_1 t} + 4D_2 t.$$

To identify water in the core of the membrane, we chose to look for water molecules that penetrated past the ether or ester oxygens of the headgroups and into the carbon-rich region. Since the membranes fluctuate in height, we did this search in a grid fashion across the full membrane surface and summed the results. The distributions of water numbers were all consistent with a Poisson process with $p$-values between 0.26 and 1 from a Kolmogorov-Smirnov test (500 data points each). The mean water per snapshot and its standard error were determined by maximum-likelihood expectation fit of the observed distribution to a Poisson distribution, again using R. Water clusters were defined as groups of two or more water molecules within the hydrophobic core that were within 5 Å of each other.

## Calculation of $H^+/OH^-$ permeability

The permeability of a membrane to a solute is defined by Eq. 1. In spherical systems such as liposomes, the flux can be related to the time derivative of the internal concentration by Eq. 3 for most solutes:

$$\frac{dC_i}{dt} = J\left(\frac{A}{V}\right) = \frac{3}{r} P_{H^+/OH^-}(C_o - C_i), \qquad (3)$$

where $A$ ($m^2$) is the membrane area, $V$ ($m^3$) is the volume of the compartment, $r$ (m) is the radius of the spherical compartment, $C_o$ (mol $m^{-3}$) is the exterior concentration, and $C_i$ (mol $m^{-3}$) is the interior concentration. However, Eq. 3 must be modified to describe protons in buffered systems (36), as protons on both sides of the membrane exist in chemical equilibrium with the protonated forms of buffering agents, fluorescent pH indicators, and lipid headgroups. The protonation or deprotonation of buffer molecules occurs on timescales much faster than that of the transport of protons across the membrane. It is therefore useful when thinking about proton flux to introduce the quantity $[H^+]_{cross}$, the net molar amount of protons that

have crossed the membrane expressed as a concentration. The governing equation of the system is then Eq. 4:

$$\frac{d[H^+]_{\text{cross}}}{dt} = \left(\frac{3P_{H^+/OH^-}}{r}\right)\left([H^+]_{f,o} - [H^+]_{f,i}\right), \quad (4)$$

where $[H^+]_{f,i}$ is the concentration of "free" protons inside the liposome. For our systems, $[H^+]_{f,o}$ is assumed to be constant during the main decay phase of the experiment, as the volume of the liposomes is vanishingly small with respect to the volume of the bulk solution.

To solve differential Eq. 4, a functional relationship between $[H^+]_{f,i}$ and $[H^+]_{\text{cross}}$ is needed. Such a function quantifies how the number of protons crossing the membrane affects the internal free proton concentration after buffering and can be obtained from the pH values gathered at each calibration jump after the liposome membranes have been permeabilized to protons via the addition of nigericin, since $[H^+]_{\text{cross}}$ at each jump is calculated from the concentrations of acid and base that have been added to the liposome solution. For example, in these experiments, $[H^+]_{\text{cross}}$ is zero before the initial acid aliquot is added and 5 mM after the addition of 2.5 mM $H_2SO_4$ and nigericin, since 5 mM $H^+$ has crossed the membrane after it has been permeabilized. Subsequently, $[H^+]_{\text{cross}}$ decreases by 1 mM after adding each calibration aliquot of 1 mM KOH. The resulting plot of $[H^+]_{f,i}$ as a function of $[H^+]_{\text{cross}}$ (Fig. 2 *B*) can be fit well ($p < 0.0001$) with an exponential growth function with fitting parameters $A_1$, $x_1$, and $y_1$ which, when inserted into Eq. 4, yields Eq. 5:

$$\frac{d[H^+]_{\text{cross}}}{dt} = \left(\frac{3P_{H^+/OH^-}}{r}\right)\left([H^+]_{f,o} - y_1 - A_1 e^{[H^+]_{\text{cross}}/x_1}\right). \quad (5)$$

Solving this ordinary differential equation for $[H^+]_{\text{cross}}(t)$ yields Eq. 6:

$$[H^+]_{\text{cross}}(t) = x_1 \ln\left(\frac{[H^+]_{f,o} - y_1}{A_1 - Ce^{\frac{3P_{H^+/OH^-}\left(y_1 - [H^+]_{f,o}\right)}{rx_1}t}}\right), \quad (6)$$

where $C$ is a constant of integration. To obtain the final fitting formula, we substitute this equation for $[H^+]_{\text{cross}}$ into the exponential decay curve with parameters $A_2$, $x_2$, and $y_2$, obtained by fitting the values of $I_{450}/I_{415}$ as a function of $[H^+]_{\text{cross}}$ obtained during calibration (Fig. 2 *C*), yielding Eq. 2.

## RESULTS AND DISCUSSION

### Attempts to optimize an assay for $H^+/OH^-$ permeability

We have adapted a fluorescence-based assay established by Paula et al. for ensemble measurements of the $H^+/OH^-$ permeability of unilamellar vesicle membranes (19). We took advantage of the ratiometric quality of pyranine, a membrane-impermeant fluorophore whose fluorescence emission intensity at 510 nm varies with pH at an excitation wavelength of 450 nm but not at an excitation wavelength of 415 nm, making it possible to control for variations in dye concentration between liposome preparations by tracking the ratio between the wavelengths rather than a raw intensity value. Rossignol et al. used this property of the dye in 1981 (37), as did Grzesiek and Dencher in 1986 (36), but most studies using pyranine since then have neglected it (7,19,26,38). Next, we developed a fitting function that makes full use of an internal calibration (19) in each experiment to minimize the assumptions we must make about buffer capacity and time-dependent changes in fluorescence intensity upon imposing a ΔpH. Although many previous studies have calculated permeability using the initial slope of the fluorescence decay curve (16,19,39), fitting with Eq. 2 allows us to make use of all the data collected and to validate the model based on quality of fit. Additionally, prior reports assumed linear buffering as pH changes (8,19,24) (often neglecting the buffering effects of lipid phosphate headgroups (36)) and made assumptions about fluorescent response to pH (19) and permeation mechanism (24) based on the fact that a single exponential function does not suffice to fit fluorescence decay curves well. Using each experiment's internal calibration, as did Paula et al. (19), enabled us to incorporate empirical measurements of the relationships between pH, buffering activity, and fluorescence intensity into the fitting function (Eq. 2), which produced excellent fits of the fluorescence decay curves after the addition of acid to the extravesicular solution ($p < 0.0001$). The permeability values we obtained for membranes from POPC and DiPhyPC lipids (Table 1) are in reasonable agreement with some literature values reported for POPC, $P_{H+/OH-} = 7 \times 10^{-5}$ cm/s (23), and for DiPhyPC, $P_{H+/OH-} = 4.0 \times 10^{-6}$ cm/s (40) and $7.0 \times 10^{-6}$ cm/s (41).

We performed all experiments in the presence of potassium ions and the $K^+$ ionophore valinomycin in solution to prevent the buildup of a membrane potential that would likely reduce the measured $H^+/OH^-$ flux (19). Previous work indicates that at high valinomycin concentrations beginning at ~100 nM, membrane $H^+/OH^-$ permeability increases sharply with increasing valinomycin concentration (16,42–44). At these elevated concentrations, valinomycin is therefore thought to display protonophoric activity in addition to ferrying $K^+$ ions (42,43,45); in 2006, Kříž et al. provided NMR evidence for the existence of an $H_3O^+$-carrying valinomycin complex, reinforcing this conclusion (46,47). We decided to experimentally establish an appropriate valinomycin concentration for the system by measuring the $H^+/OH^-$ permeability of POPC vesicles at different valinomycin concentrations. Our goal was to find a range in which liposomes would exhibit $P_{H+/OH-}$ values higher than in the absence of valinomycin, indicating that the buildup of a membrane potential accompanying $H^+$ diffusion was being successfully prevented via $K^+$ diffusion, but in which $P_{H+/OH-}$ was independent of the valinomycin concentration, since a positive dependence would indicate protonophoric activity. As valinomycin is poorly soluble in water, we added it to liposome solutions via concentrated aliquots in DMSO; the resulting plot of $P_{H+/OH-}$ versus valinomycin concentration is shown in Fig. 3. We chose DMSO as a solvent rather than ethanol (used in Paula et al. (19)), because DMSO has a smaller effect on $P_{H+/OH-}$ (Fig. 3, *leftmost data points*). The $H^+/OH^-$

**TABLE 1 Comparison of Lipids Examined in This Work**

| Lipid | Thickness (nm) | | Area per Lipid (Å$^2$)[a] | Variance in Area per Lipid (Å$^2$)[a] | $D_1$ ($\times 10^{-11}$ m$^2$/s)[a] | $D_2$ ($\times 10^{-11}$ m$^2$/s)[a] | $D_L$ ($\times 10^{-13}$ m$^2$/s) (± SE) | Entropy (J mol$^{-1}$ K$^{-1}$)[a] | Bending Rigidity (pN nm)[a] | $P_{H+/OH-}$ ($\times 10^{-6}$ cm/s) (95% CI) |
|---|---|---|---|---|---|---|---|---|---|---|
| | MD | AFM | | | | | | | | |
| T28 | 3.78 ± 0.01 | 4.4 ± 0.01 | 63.7 ± 0.02 | 0.047 ± 0.005 | 2.03 ± 0.10 | 0.13 ± 0.004 | 0.6 ± 0.2 | 5080 ± 22 | 5470 | 6.2 (1.3–11.0) |
| T32 | 4.01 ± 0.01 | ND | 63.1 ± 0.01 | 0.360 ± 0.004 | 2.22 ± 0.17 | 0.16 ± 0.004 | 0.6 ± 0.1 | 5276 ± 20 | 3960 | 11.8 (3.6–20.0) |
| T36 | 4.11 ± 0.02 | 4.6 ± 0.01 | 64.4 ± 0.02 | 0.063 ± 0.006 | 1.88 ± 0.09 | 0.12 ± 0.004 | 0.5 ± 0.2 | 5481 ± 20 | 4510 | 26.3 (8.8–43.9) |
| U16 | 3.81 ± 0.02 | ND | 69.0 ± 0.02 | 0.090 ± 0.009 | 2.99 ± 0.14 | 0.42 ± 0.003 | 9.4 ± 1.1 | 5565 ± 17[b] | 4060 | 7.7 (3.8–11.7) |
| Di-O-PhyPC | ND | ND | ND | | ND | ND | 2.9 ± 0.5 | ND | ND | 4.0 (−1.8–9.7) |
| DiPhyPC | 3.78 ± 0.03 | Lit: 5.3 (50) | 78.6 ± 0.06 Lit: 80.6 (52) | 0.193 ± 0.039 | 2.45 ± 0.10 | 0.21 ± 0.004 | 5.7 ± 0.5 | 5459 ± 18[b] | 4470 | 2.8 (0.5–5.1) |
| POPC | 3.96 ± 0.02 | Lit: 4.6 (51) | 64.2 ± 0.03 Lit: 64.3 (52) | 0.213 ± 0.021 | 4.65 ± 0.14 | 0.65 ± 0.002 | 12.0 ± 1.5 | 5531 ± 14[b] | 2670 | 10.6 (4.5–16.8) |

Except in the case of bending rigidity and $P_{H+/OH-}$ (last two columns), values are expressed as the mean ± SE. ND, not done; CI, confidence interval.
[a]Unless otherwise indicated, these values were obtained from MD simulations.
[b]The entropy values of untethered lipids U16, DiPhyPC, and POPC were multiplied by 2 for comparison to the tethered lipids.

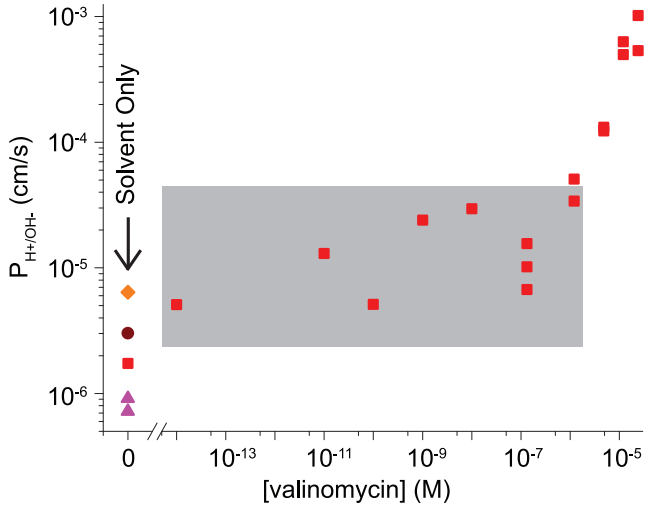


FIGURE 3 Valinomycin concentrations up to $10^{-7}$ M prevent membrane potential buildup without causing an increase in $P_{H+/OH-}$. Before the axis break, points represent $P_{H+/OH-}$ after the addition of the solvent vehicle only as indicated by the symbols: red squares, 2.66 μL DMSO; brown circle, 1.33 μL ethanol; orange diamond, 2.66 μL ethanol; pink triangles, no solvent. After the axis break, the final concentration of valinomycin indicated on the *x* axis was added in 2.66 μL DMSO to a total volume of 1 mL. Red squares within the area shaded in gray represent data within the "plateau" range of valinomycin concentrations. All experiments were run on POPC vesicles extruded through filters with an 80 nm pore diameter. To see this figure in color, go online.

permeability increased from the baseline value after the addition of just 10 fM valinomycin and plateaued with increasing valinomycin concentrations until a point of inflection was reached around 100 nM, at which point $P_{H+/OH-}$ began to increase dramatically in the presence of more valinomycin. We selected a valinomycin concentration of 10 nM for all subsequent experiments.

## Systematic variation of a series of archaea-inspired lipids

We explored the effect of transmembrane tethering, tether length, and the presence of isoprenoid methyl groups on one or both lipid tails on the $P_{H+/OH-}$ values through liposomes formed from a series of synthetic lipids with small systematic structural variations. T28, T32, and T36 have an unbranched, saturated alkyl tether linked via ether bonds to two glycerophosphocholine headgroups that each have one phytanyl tail of 16 carbons (Fig. 1, *A–C*). The lipid U16 (Fig. 1 *D*) is untethered and has a 16-carbon straight chain attached to the headgroup in place of the tether; it is structurally equivalent to half of T32. The commercially available lipid Di-O-PhyPC (Fig. 1 *E*) differs from U16 only insofar as it has two phytanyl chains instead of one phytanyl and one *n*-alkane acyl chain. DiPhyPC (Fig. 1 *F*) is identical to Di-O-PhyPC except that the phytanyl chains are attached to the headgroups with ester rather than ether linkages. Fig. 4 compares $H^+/OH^-$ permeability

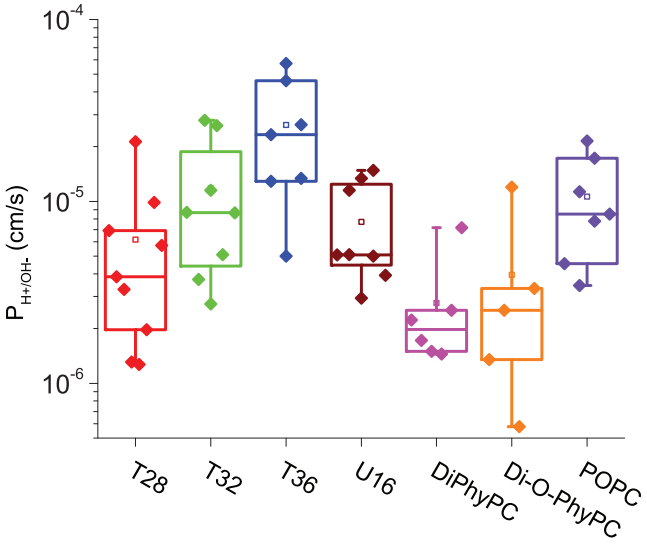


FIGURE 4 Box-and-whisker plots showing $P_{H+/OH-}$ values gathered from seven different lipids. The whiskers extend to the minimal and maximal values, the box covers the interquartile range, the center line represents the median, and the open square represents the mean. To see this figure in color, go online.

values for tethered and untethered archaea-inspired lipids alongside those gathered for POPC (Fig. 1 *G*).

## $H^+/OH^-$ permeability of tethered lipids increases with tether length

The $P_{H+/OH-}$ permeability results from the lipids T28, T32, and T36 indicate that liposome membranes become more permeable to protons as tether length increases if the length of the untethered acyl chain is kept constant (Table 1). A Tukey honest significant difference test comparing the log-transformed $P_{H+/OH-}$ values of these three lipids found the mean $H^+/OH^-$ permeability of liposomes composed of T28 lipids to be significantly smaller ($p = 0.01$) than that of T36 liposomes. As in prior research studies (19), we used log-transformed values for all statistical comparisons, because the populations of measured $P_{H+/OH-}$ values failed tests of homogeneity of variance (Levene's, $p = 0.002$; Brown-Forsythe, $p = 0.02$) unless the values were log-transformed (Levene's, $p = 0.72$; Brown-Forsythe, $p = 0.75$).

## Results from MD simulations

In an attempt to gain insight into the molecular differences that may affect proton permeability through membranes, we conducted MD simulations of membranes composed of each lipid (except Di-O-PhyPC) to measure structural parameters such as membrane thickness, area per lipid, lateral diffusion coefficients, conformational entropy, and bending rigidity. Table 1 shows the results from MD simulations for these lipids; they agree well with experimentally measured values. For instance, the lateral diffusion coefficients $D_2$ determined by MD simulations were strongly correlated with lateral diffusion coefficients ($D_L$) measured by fluorescence recovery after photobleaching (FRAP) experiments on supported lipid bilayers of the same six lipids (Table 1, Pearson correlation coefficient, $r = 0.95$ with $p = 0.004$). Additionally, the thicknesses of T28 and T32 membranes as measured by atomic force microscopy (AFM) were 0.5 to 0.6 nm larger than those determined by MD, which falls within the literature range for the thickness of the expected water layer between lipids and the underlying mica substrate used for AFM measurements (0.4–1.7 nm) (Fig. S1) (48,49). Previous studies that compared bilayer thickness defined by AFM for POPC and DiPhyPC with the MD data also reported water layer thicknesses in this range (Table 1) (50,51). Further, the area-per-lipid values obtained from MD for POPC and DiPhyPC are within 3% of literature values obtained by Kučerka et al. from small-angle x-ray and neutron scattering (52).

The experimentally measured $H^+/OH^-$ permeability in monolayers of tethered lipids increased with increasing tether length (T28, T32, and T36). The results from MD simulations, reported in Table 1, reveal that membrane stiffness decreases and lipid entropy increases with increasing lipid tether length, as well. Shinoda et al. and Haines each propose that crowding in the hydrocarbon core of membranes reduces proton leakage (53,54). In the tethered lipids, the two untethered phytanyl chains have a combined length of 32 methylene groups—four carbons longer than the T28 tether and four carbons shorter than the T36 tether; the differences in $P_{H+/OH-}$ may be attributable to increased hydrocarbon crowding in T28 and the presence of a "gap" in T36. Therefore, the observed reduction in proton permeability in the sequence of membranes from T36 lipids to T32 lipids to T28 lipids could be a result of the increasing crowding, order, and stiffness of the hydrophobic region of the membranes.

MD simulations also reveal that despite the hydrophobic nature of the membrane core, water molecules regularly enter this region, as found previously in the literature (55–60) (see Fig. S2). Defining a penetration event as an instance when a water molecule moves past the ether or ester oxygen of the nearest lipid into the hydrophobic region, we found penetration frequencies of $8 \times 10^{-3}$ to $1.6 \times 10^{-2}$ $nm^{-2}$ $ns^{-1}$. These values are similar to the water penetration frequencies reported by Krylov et al. from MD simulations of DOPS, DPPC, and DOPC membranes, which ranged from $3.5 \times 10^{-3}$ to $4.3 \times 10^{-2}$ $nm^{-2}$ $ns^{-1}$ (60). (We note that this discussion is limited to the penetration of water molecules into the hydrophobic region of the membrane rather than water permeation all the way through the bilayer.) The number of water molecules is consistent with a Poisson process, implying that the entry of a given water molecule is independent from that of other water molecules. Quantifying the entry of water

molecules into the hydrophobic core in all six simulated membranes (including three untethered lipids, Table 2) revealed that log $P_{H+/OH-}$ correlated with the total number of water molecules that spontaneously entered the membrane over 50 ns (Pearson coefficient, $r = 0.86$; $p = 0.027$). A better correlation was found between log $P_{H+/OH-}$ and the number of observations with at least three water molecules residing anywhere in the hydrophobic core of the membrane (Pearson coefficient, $r = 0.99$; $p = 0.0003$; Fig. 5 *A*).

Although we would not expect the distribution of water molecules to be uniform throughout the volume of the hydrophobic core of the lipid membrane (the probability should fall off with increasing distance from the headgroup into the core (60)), it should be roughly uniform across the surface area of the membrane. Thus, the probability of finding two water molecules in the vicinity of the same lipid headgroup would be inversely proportional to the number of headgroups, which for all of our simulated membranes would be 1/1458 or ~0.07%. If we take the T28 membrane as an example, we find 59 instances of 2 or more water molecules anywhere in the membrane in our simulations (data taken at 0.1 ns intervals over 50 ns, i.e., 500 observations); this value approximates the expected value of 63.3 from the corresponding best-fit Poisson distribution. Interestingly, in 17 of these 59 instances, water molecules were located within 5 Å of each other; we define this condition as a water cluster. This observed clustering probability of 28% is well above the expected 0.07%, leading us to conclude that although water molecules appear to enter the hydrophobic core independently, they have a strong tendency to cluster after entry. As shown in Fig. 5 *B*, the number of observed water clusters also correlates well (Pearson coefficient, $r = 0.88$; $p = 0.022$) with the measured proton permeability; this observation is consistent with prior observations in the literature (18,39,54,61).

Indeed, the formation of water chains or clusters is thought to be a primary mechanism for proton shuttling across the membrane (53), and although our simulations were not long enough to capture water chains that span the entire membrane thickness, we do see the formation of nascent clusters with multiple water molecules (Fig. 5 *C*). Previous MD simulations made similar observations and ultimately concluded that the clustering of water molecules is relevant for the permeation of protons but not water and that the presence of phytanyl groups would serve to disrupt water clusters and decrease proton permeability (54). Experimental studies using FTIR spectrometry similarly found that the formation of water clusters within the membrane depended strongly on the acyl chain composition (62). Taken together, these results support the idea that water entry and clustering in the hydrophobic core are both relevant metrics for proton permeation. We caution, however, that although the likelihood that this correlation was a result of random chance is very low, this relationship will have to be tested with additional lipids, given the large uncertainty in the measured proton permeabilities and the limited number of six data pairs in the correlation analysis. We are currently trying to expand the number of tested lipids, however, the synthesis of archaea-inspired lipids is extremely work intensive, and MD simulations are time intensive, requiring a separate follow-up study.

## Tethered and untethered lipids are equally $H^+/OH^-$ permeable at room temperature

Interestingly, tethering itself did not seem to affect $H^+/OH^-$ permeability in our measurements. To observe the effects of tethering, we compared $P_{H+/OH-}$ values from membranes composed of U16 and T32, since T32's structure is identical to two U16 lipids bonded together at the terminal carbons of their unbranched chains (Fig. 1, *B* and *D*). A two-tailed Student's *t*-test comparing the log-transformed permeability values of T32 and U16 vesicles (Table 1) showed that they were not significantly different ($p = 0.46$); the spread of the U16 $P_{H+/OH-}$ values fell entirely within the spread of the T32 $P_{H+/OH-}$ values. It is worth noting, however, that we conducted all our experiments at room temperature. Komatsu and Chong found that the $H^+/OH^-$ permeability of doubly tethered lipids isolated from *Sulfolobus acidocaldarius* was relatively invariant with respect to temperature from 25 to 80°C, whereas $P_{H+/OH-}$ values from standard (untethered) eggPC lipids increased dramatically with increasing temperature. The $P_{H+/OH-}$ values from the two membrane compositions

**TABLE 2 Observation of Water Molecules in the Hydrophobic Core of Lipid Membranes as Determined by MD Simulations over 50 ns**

| Lipid | Total No. of Water Molecules Observed in Membrane | Mean No. of Water Molecules per Snapshot ± SE | No. of Observations with at Least Three Water Molecules Anywhere in the Membrane | No. of Clusters with Two or More Water Molecules |
|---|---|---|---|---|
| T28 | 307 | 0.614 ± 0.035 | 16 | 17 |
| T32 | 349 | 0.698 ± 0.037 | 25 | 26 |
| T36 | 374 | 0.748 ± 0.039 | 31 | 29 |
| U16 | 346 | 0.692 ± 0.037 | 20 | 20 |
| DiPhyPC | 230 | 0.460 ± 0.030 | 6 | 18 |
| POPC | 391 | 0.782 ± 0.040 | 24 | 26 |

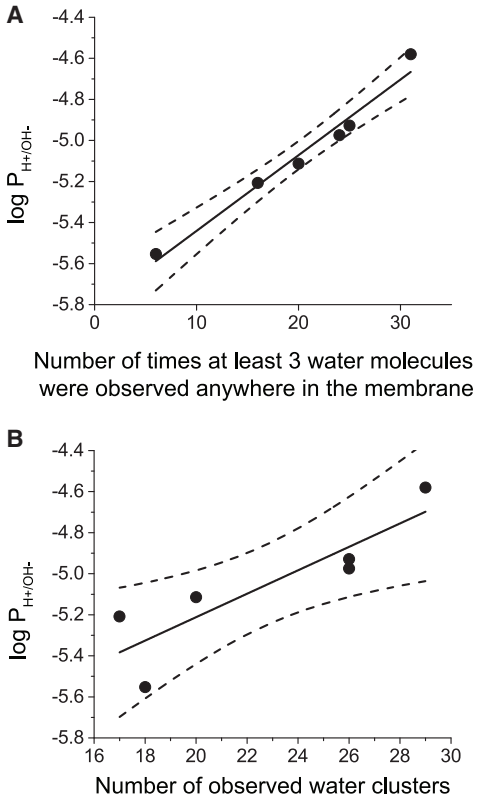


FIGURE 5 Water within the hydrophobic region is predictive of log $P_{H+/OH-}$. (*A*) Correlation plot of log $P_{H+/OH-}$ as a function of the number of times at least three water molecules simultaneously occupied the hydrophobic region anywhere in the lipid membrane over the course of a 50 ns MD simulation. The Pearson coefficient is $r = 0.99$. The solid line is the best fit to a straight line; dotted lines show the 95% confidence interval from the fit. (*B*) Correlation plot of log $P_{H+/OH-}$ as a function of the number of times a water cluster appeared in the hydrophobic region of the lipid membrane over the course of a 50 ns MD simulation. The Pearson coefficient is $r = 0.88$. (*C*) A snapshot from the MD simulation of a membrane from T28 lipids, showing the penetration of water molecules into the hydrophobic core of the membrane. Water molecules are shown as van der Waals spheres and the solvent-accessible surface area around the waters in the membrane core is shown in blue. To see this figure in color, go online.

were comparable at room temperature but diverged greatly at higher temperatures (63).

### Isoprenoid methyls decrease $H^+/OH^-$ permeability

Based on a two-tailed Student's *t*-test comparing log-transformed $P_{H+/OH-}$ values, the mean permeability of liposomes from Di-O-PhyPC lipids was lower ($p = 0.059$) than that from U16 lipids (Table 1). Given that U16 and Di-O-PhyPC only differ structurally by the presence or absence of isoprenoid methyl groups on one lipid tail, this result agrees with previous findings that this motif lowers $H^+/OH^-$ permeability (8). Most lipids characteristic of acidophilic archaea display the isoprenoid methyl motif on both acyl chains (1).

### Possible reasons for variability in measured $P_{H+/OH-}$ values

Despite strong efforts to optimize the permeability assay, we were unable to eliminate variability between measured $H^+/OH^-$ permeability values of membranes composed of the same lipid. This variability, seen both in this work and in the literature (8,16,21,25,37,41,64,65), represents a limitation of the usefulness of $P_{H+/OH-}$ data (24,26). We have attempted to identify and minimize potential sources of variation inherent in the process of gathering $P_{H+/OH-}$ values, and we present a detailed discussion on this topic in Section S2 of the Supporting Material.

## CONCLUSIONS

We have optimized a fluorescence-based $H^+/OH^-$ permeability assay by introducing a fitting formula that describes the entire kinetics of a step ΔpH-induced change of the interior pH of liposomes and by establishing an appropriate concentration of valinomycin (10 nM) to investigate permeability values in homogeneous lipid membranes containing synthetic archaea-inspired lipids. The lipid T32, which was tethered by a straight 32-carbon chain, produced membranes with $P_{H+/OH-}$ values similar to those of membranes composed of its untethered equivalent, U16, revealing that tethering does not affect $P_{H+/OH-}$ at room temperature. However, $P_{H+/OH-}$ values among tethered lipid membranes increased with increasing tether length if the number of carbons in the untethered acyl tail was constant. Further, monopolar lipids with two tails containing isoprenoid methyl branches form membranes with lower $H^+/OH^-$ permeability than those with one branching tail and one unbranched tail. In addition, MD simulations carried out in this work suggest that the penetration of water into the hydrophobic core of lipid membranes predicts their proton permeability. These results inform the design of synthetic bipolar lipid molecules for desired $H^+/OH^-$ permeability characteristics.

## SUPPORTING MATERIAL

Supporting Materials and Methods, Supporting Discussion, and eight figures are available at http://www.biophysj.org/biophysj/supplemental/S0006-3495(16)30247-8.

## AUTHOR CONTRIBUTIONS

T.B.H.S. and M.M. conceived and designed the permeability experiments. G.L. and T.K. synthesized the lipids. T.B.H.S., M.A.J., K.N.H., and C.L.W. performed permeability experiments. O.M.E. performed lateral diffusion experiments. Y.H.K. performed atomic force microscopy. K.D. and D.S. designed and performed the molecular dynamics experiments. J.Y. designed the lipid synthesis. T.B.H.S., K.D., D.S., and M.M. contributed analysis. T.B.H.S., G.L., D.S., J.Y., and M.M. wrote the article.

## ACKNOWLEDGMENTS

We thank the laboratory of Prof. Mary-Ann Mycek for the use of their spectrofluorometer.

Research reported in this publication was supported by the Air Force Office of Scientific Research (grant no. FA9550-12-1-0435 to M.M., J.Y., and D.S.) and the National Institute of General Medical Sciences of the National Institutes of Health under award number T32GM008353 (T.B.H.S.). The content is solely the responsibility of the authors and does not necessarily represent the official views of the National Institutes of Health.

## SUPPORTING CITATIONS

References (66–75) appear in the Supporting Material.

## REFERENCES

1. Ulrih, N. P., D. Gmajner, and P. Raspor. 2009. Structural and physicochemical properties of polar lipids from thermophilic archaea. *Appl. Microbiol. Biotechnol.* 84:249–260.
2. Schleper, C., G. Puehler, …, W. Zillig. 1995. *Picrophilus* gen. nov., fam. nov.: a novel aerobic, heterotrophic, thermoacidophilic genus and family comprising archaea capable of growth around pH 0. *J. Bacteriol.* 177:7050–7059.
3. Konings, W. N., S.-V. Albers, …, A. J. M. Driessen. 2002. The cell membrane plays a crucial role in survival of bacteria and archaea in extreme environments. *Antonie van Leeuwenhoek.* 81:61–72.
4. Baker-Austin, C., and M. Dopson. 2007. Life in acid: pH homeostasis in acidophiles. *Trends Microbiol.* 15:165–171.
5. Michels, M., and E. P. Bakker. 1985. Generation of a large, protonophore-sensitive proton motive force and pH difference in the acidophilic bacteria *Thermoplasma acidophilum* and *Bacillus acidocaldarius*. *J. Bacteriol.* 161:231–237.
6. Tyson, G. W., J. Chapman, …, J. F. Banfield. 2004. Community structure and metabolism through reconstruction of microbial genomes from the environment. *Nature.* 428:37–43.
7. Elferink, M. G. L., J. G. de Wit, …, W. N. Konings. 1994. Stability and proton-permeability of liposomes composed of archaeal tetraether lipids. *Biochim. Biophys. Acta.* 1193:247–254.
8. Mathai, J. C., G. D. Sprott, and M. L. Zeidel. 2001. Molecular mechanisms of water and solute transport across archaebacterial lipid membranes. *J. Biol. Chem.* 276:27266–27271.
9. De Rosa, M., A. Gambacorta, …, P. Albrecht. 1983. Isoprenoid ethers; backbone of complex lipids of the archaebacterium *Sulfolobus solfataricus*. *Biochim. Biophys. Acta.* 753:249–256.
10. Sprott, G. D., M. Meloche, and J. C. Richards. 1991. Proportions of diether, macrocyclic diether, and tetraether lipids in *Methanococcus jannaschii* grown at different temperatures. *J. Bacteriol.* 173:3907–3910.
11. Lai, D., J. R. Springstead, and H. G. Monbouquette. 2008. Effect of growth temperature on ether lipid biochemistry in *Archaeoglobus fulgidus*. *Extremophiles.* 12:271–278.
12. De Rosa, M., E. Esposito, …, J. D. Bu'Lock. 1980. Effects of temperature on ether lipid composition of *Caldariella acidophila*. *Phytochemistry.* 19:827–831.
13. Uda, I., A. Sugai, …, T. Itoh. 2004. Variation in molecular species of core lipids from the order *Thermoplasmales* strains depends on the growth temperature. *J. Oleo Sci.* 53:399–404.
14. de Grotthuss, C. J. T. 2006. Memoir on the decomposition of water and of the bodies that it holds in solution by means of galvanic electricity. 1805. *Biochim. Biophys. Acta.* 1757:871–875.
15. Cukierman, S. 2006. Et tu, Grotthuss! and other unfinished stories. *Biochim. Biophys. Acta.* 1757:876–885.
16. Nichols, J. W., and D. W. Deamer. 1980. Net proton-hydroxyl permeability of large unilamellar liposomes measured by an acid-base titration technique. *Proc. Natl. Acad. Sci. USA.* 77:2038–2042.
17. Nagle, J. F. 1987. Theory of passive proton conductance in lipid bilayers. *J. Bioenerg. Biomembr.* 19:413–426.
18. Deamer, D. W., and J. W. Nichols. 1989. Proton flux mechanisms in model and biological membranes. *J. Membr. Biol.* 107:91–103.
19. Paula, S., A. G. Volkov, …, D. W. Deamer. 1996. Permeation of protons, potassium ions, and small polar molecules through phospholipid bilayers as a function of membrane thickness. *Biophys. J.* 70:339–348.
20. Nichols, J. W., and R. F. Abercrombie. 2010. A view of hydrogen/hydroxide flux across lipid membranes. *J. Membr. Biol.* 237:21–30.
21. Lande, M. B., J. M. Donovan, and M. L. Zeidel. 1995. The relationship between membrane fluidity and permeabilities to water, solutes, ammonia, and protons. *J. Gen. Physiol.* 106:67–84.
22. Gensure, R. H., M. L. Zeidel, and W. G. Hill. 2006. Lipid raft components cholesterol and sphingomyelin increase $H^+/OH^-$ permeability of phosphatidylcholine membranes. *Biochem. J.* 398:485–495.
23. Deamer, D. W., and J. W. Nichols. 1983. Proton-hydroxide permeability of liposomes. *Proc. Natl. Acad. Sci. USA.* 80:165–168.
24. Kuyper, C. L., J. S. Kuo, …, D. T. Chiu. 2006. Proton permeation into single vesicles occurs via a sequential two-step mechanism and is heterogeneous. *J. Am. Chem. Soc.* 128:3233–3240.
25. Perkins, W. R., and D. S. Cafiso. 1986. An electrical and structural characterization of proton/hydroxide currents in phospholipid vesicles. *Biochemistry.* 25:2270–2276.
26. van de Vossenberg, J. L. C. M., A. J. M. Driessen, …, W. N. Konings. 1999. Homeostasis of the membrane proton permeability in *Bacillus subtilis* grown at different temperatures. *Biochim. Biophys. Acta.* 1419:97–104.
27. Hope, M. J., M. B. Bally, …, P. R. Cullis. 1985. Production of large unilamellar vesicles by a rapid extrusion procedure: characterization of size distribution, trapped volume and ability to maintain a membrane potential. *Biochim. Biophys. Acta.* 812:55–65.
28. Mingeot-Leclercq, M.-P., M. Deleu, …, Y. F. Dufrêne. 2008. Atomic force microscopy of supported lipid bilayers. *Nat. Protoc.* 3:1654–1659.
29. Lee, J., A. L. Gillman, …, F. Teran Arce. 2014. Role of the fast kinetics of pyroglutamate-modified amyloid-$\beta$ oligomers in membrane binding and membrane permeability. *Biochemistry.* 53:4704–4714.
30. Richter, R. P., and A. R. Brisson. 2005. Following the formation of supported lipid bilayers on mica: a study combining AFM, QCM-D, and ellipsometry. *Biophys. J.* 88:3422–3433.
31. Humphrey, W., A. Dalke, and K. Schulten. 1996. VMD: visual molecular dynamics. *J. Mol. Graph.* 14:33–38, 27–28.
32. Phillips, J. C., R. Braun, …, K. Schulten. 2005. Scalable molecular dynamics with NAMD. *J. Comput. Chem.* 26:1781–1802.

33. Watson, M. C., E. S. Penev, …, F. L. H. Brown. 2011. Thermal fluctuations in shape, thickness, and molecular orientation in lipid bilayers. *J. Chem. Phys.* 135:244701.

34. Schlitter, J. 1993. Estimation of absolute and relative entropies of macromolecules using the covariance matrix. *Chem. Phys. Lett.* 215:617–621.

35. Wohlert, J., and O. Edholm. 2006. Dynamics in atomistic simulations of phospholipid membranes: nuclear magnetic resonance relaxation rates and lateral diffusion. *J. Chem. Phys.* 125:204703.

36. Grzesiek, S., and N. A. Dencher. 1986. Dependency of ΔpH-relaxation across vesicular membranes on the buffering power of bulk solutions and lipids. *Biophys. J.* 50:265–276.

37. Rossignol, M., P. Thomas, and C. Grignon. 1982. Proton permeability of liposomes from natural phospholipid mixtures. *Biochim. Biophys. Acta.* 684:195–199.

38. Clement, N. R., and J. M. Gould. 1981. Pyranine (8-hydroxy-1,3,6-pyrenetrisulfonate) as a probe of internal aqueous hydrogen ion concentration in phospholipid vesicles. *Biochemistry.* 20:1534–1538.

39. Ira, and G. Krishnamoorthy. 2001. Probing the link between proton transport and water content in lipid membranes. *J. Phys. Chem. B.* 105:1484–1488.

40. Gutknecht, J. 1987. Proton/hydroxide conductance and permeability through phospholipid bilayer membranes. *Proc. Natl. Acad. Sci. USA.* 84:6443–6446.

41. Yamauchi, K., K. Doi, …, M. Kinoshita. 1993. Archaebacterial lipids: highly proton-impermeable membranes from 1,2-diphytanyl-*sn*-glycero-3-phosphocholine. *Biochim. Biophys. Acta.* 1146:178–182.

42. Brookes, P. S., D. F. S. Rolfe, and M. D. Brand. 1997. The proton permeability of liposomes made from mitochondrial inner membrane phospholipids: comparison with isolated mitochondria. *J. Membr. Biol.* 155:167–174.

43. Seigneuret, M., and J. L. Rigaud. 1986. Analysis of passive and light-driven ion movements in large bacteriorhodopsin liposomes reconstituted by reverse-phase evaporation. 1. Factors governing the passive proton permeability of the membrane. *Biochemistry.* 25:6716–6722.

44. Brand, M. D., P. Couture, and A. J. Hulbert. 1994. Liposomes from mammalian liver mitochondria are more polyunsaturated and leakier to protons than those from reptiles. *Comp. Biochem. Physiol. B.* 108:181–188.

45. Pennisi, C. P., E. Greenbaum, and K. Yoshida. 2010. Analysis of light-induced transmembrane ion gradients and membrane potential in Photosystem I proteoliposomes. *Biophys. Chem.* 146:13–24.

46. Kríz, J., J. Dybal, and E. Makrlík. 2006. Valinomycin-proton interaction in low-polarity media. *Biopolymers.* 82:536–548.

47. Kríz, J., E. Makrlík, and P. Vaňura. 2006. NMR evidence of a valinomycin-proton complex. *Biopolymers.* 81:104–109.

48. Miller, C. E., J. Majewski, …, T. L. Kuhl. 2005. Characterization of biological thin films at the solid-liquid interface by x-ray reflectivity. *Phys. Rev. Lett.* 94:238104.

49. Bayerl, T. M., and M. Bloom. 1990. Physical properties of single phospholipid bilayers adsorbed to micro glass beads. A new vesicular model system studied by $^{2}$H-nuclear magnetic resonance. *Biophys. J.* 58:357–362.

50. Garavaglia, M., S. Dopinto, …, M. Paulmichl. 2004. Membrane thickness changes ion-selectivity of channel-proteins. *Cell. Physiol. Biochem.* 14:231–240.

51. Åkesson, A., T. Lind, …, M. Cárdenas. 2012. Composition and structure of mixed phospholipid supported bilayers formed by POPC and DPPC. *Soft Matter.* 8:5658–5665.

52. Kučerka, N., M.-P. Nieh, and J. Katsaras. 2011. Fluid phase lipid areas and bilayer thicknesses of commonly used phosphatidylcholines as a function of temperature. *Biochim. Biophys. Acta.* 1808:2761–2771.

53. Haines, T. H. 2001. Do sterols reduce proton and sodium leaks through lipid bilayers? *Prog. Lipid Res.* 40:299–324.

54. Shinoda, W., M. Mikami, …, M. Hato. 2004. Molecular dynamics study on the effects of chain branching on the physical properties of lipid bilayers: 2. Permeability. *J. Phys. Chem. B.* 108:9346–9356.

55. Finkelstein, A. 1987. Water Movement through Lipid Bilayers, Pores, and Plasma Membranes: Theory and Reality. Wiley, New York.

56. Haines, T. H. 1994. Water transport across biological membranes. *FEBS Lett.* 346:115–122.

57. Ollila, S., M. T. Hyvönen, and I. Vattulainen. 2007. Polyunsaturation in lipid membranes: dynamic properties and lateral pressure profiles. *J. Phys. Chem. B.* 111:3139–3150.

58. Orsi, M., D. Y. Haubertin, …, J. W. Essex. 2008. A quantitative coarse-grain model for lipid bilayers. *J. Phys. Chem. B.* 112:802–815.

59. Orsi, M., J. Michel, and J. W. Essex. 2010. Coarse-grain modelling of DMPC and DOPC lipid bilayers. *J. Phys. Condens. Matter.* 22:155106.

60. Krylov, N. A., V. M. Pentkovsky, and R. G. Efremov. 2013. Nontrivial behavior of water in the vicinity and inside lipid bilayers as probed by molecular dynamics simulations. *ACS Nano.* 7:9428–9442.

61. Elamrani, K., and A. Blume. 1983. Effect of the lipid phase transition on the kinetics of $H^{+}/OH^{-}$ diffusion across phosphatidic acid bilayers. *Biochim. Biophys. Acta.* 727:22–30.

62. Disalvo, E. A., A. M. Bouchet, and M. A. Frias. 2013. Connected and isolated $CH_2$ populations in acyl chains and its relation to pockets of confined water in lipid membranes as observed by FTIR spectrometry. *Biochim. Biophys. Acta.* 1828:1683–1689.

63. Komatsu, H., and P. L. Chong. 1998. Low permeability of liposomal membranes composed of bipolar tetraether lipids from thermoacidophilic archaebacterium *Sulfolobus acidocaldarius*. *Biochemistry.* 37:107–115.

64. Paula, S. 2014. An introduction to passive ion transport across model lipid membranes for undergraduate students: proton permeation measurements in liposomes. *J. Chem. Educ.* 91:145–148.

65. Paxton, W. F., D. Price, and N. J. Richardson. 2013. Hydroxide ion flux and pH-gradient driven ester hydrolysis in polymer vesicle reactors. *Soft Matter.* 9:11295–11302.

66. Hope, M. J., M. B. Bally, …, P. R. Cullis. 1986. Generation of multilamellar and unilamellar phospholipid vesicles. *Chem. Phys. Lipids.* 40:89–107.

67. De Rosa, M., A. Gambacorta, and B. Nicolaus. 1983. A new type of cell membrane, in thermophilic archaebacteria, based on bipolar ether lipids. *J. Membr. Sci.* 16:287–294.

68. Koyanagi, T., G. Leriche, …, J. Yang. 2016. Cyclohexane rings reduce membrane permeability to small ions in archaea-inspired tetraether lipids. *Angew. Chem. Int. Ed. Engl.* 55:1890–1893.

69. Wagner, A., M.-P. Heitz, and C. Mioskowski. 1989. Direct conversion of tetrahydropyranylated alcohols to the corresponding bromides. *Tetrahedron Lett.* 30:557–558.

70. Chung, Y. C., Y. H. Chiu, …, Y. T. Tao. 2005. Self-assembled biomimetic monolayers using phospholipid-containing disulfides. *Biomaterials.* 26:2313–2324.

71. Febo-Ayala, W., S. L. Morera-Félix, …, D. H. Thompson. 2006. Functional reconstitution of the integral membrane enzyme, isoprenylcysteine carboxyl methyltransferase, in synthetic bolalipid membrane vesicles. *Biochemistry.* 45:14683–14694.

72. Babu, K. V., and G. V. M. Sharma. 2008. Total synthesis of patulolide C and 11-epipatulolide C. *Tetrahedron Asymmetry.* 19:577–583.

73. Gao, Y., J. Z. Vlahakis, …, I. Brockhausen. 2013. Selective inhibition of glycosyltransferases by bivalent imidazolium salts. *Bioorg. Med. Chem.* 21:1305–1311.

74. Shirouzu, T., K. Watari, …, T. Miyamoto. 2013. Structure, synthesis, and biological activity of a C-20 bisacetylenic alcohol from a marine sponge *Callyspongia* sp. *J. Nat. Prod.* 76:1337–1342.

75. Mangaleswaran, S., and N. P. Argade. 2001. A facile synthesis of naturally occurring aminopeptidase inhibitor tyromycin A. *J. Org. Chem.* 66:5259–5261.